Evaluating Ocean Tide Models Using Absolute Gravity Measurements at Aboa, Dronning Maud Land, Antarctica

Arttu Raja-Halli, Jaakko Mäkinen, Jyri Näränen, and Maaria Nordman

Abstract

Accurate modeling of ocean tidal loading (OTL) is essential for geodetic data analysis, allowing isolation of other geophysical signals such as ice mass changes and glacial isostatic adjustment (GIA). Modeling OTL in the Antarctic region is challenging due to sparse observations, poorly constrained sub-ice topography, and complex grounding line dynamics. We use absolute gravity (AG) measurements from the Finnish Antarctic station Aboa (Dronning Maud Land) to evaluate several global and regional ocean tide models. Two AG campaigns in January–February 2024 (each ~6 days) reveal OTL amplitudes of up to 20 μGal (2×10^{-7} m/s^2) peak-to-peak, providing the first comparison of absolute gravity measurements and OTL models in the Western Dronning Maud Land. Synthetic OTL time series were computed for global models FES2004, FES2022b, DTU23, EOT20, TPXO10-atlas-v2, and the regional CATS2008v2023 model, and compared directly with AG measurements. The modelled loadings were subtracted from the AG measurements to quantify model misfit and identify which model minimizes the residual gravity variability. Because of the limited observation duration, the analysis focuses on diurnal and semidiurnal tidal constituents. Comparisons show that differences between models in predicted loading primarily originate within a ~200 km radius around Aboa. All models provide adequate correction to the AG time series, with inter-model differences below the AG measurement uncertainty. These results suggest that, while current global models already perform well for OTL corrections at Aboa, the inclusion of regional Antarctic model CATS2008v2023 helps to constrain local tidal dynamics and improves confidence in gravimetric studies in coastal Antarctica.

Keywords

Absolute gravity · Antarctica · Ocean tidal loading

1 Introduction

Absolute gravity (AG) measurements react to temporal variations in the Earth's gravity field, which reflect the combined effects of mass redistributions and vertical crustal motion. AG can be used to distinguish the changes due to glacial isostatic adjustment (GIA) of the Holocene deglaciation and present-day ice mass changes (Bilker-Koivula et al. 2021; van Dam et al. 2017). Accurate GIA modelling is essential for reliably estimating Antarctica's ice mass balance and its

A. Raja-Halli (✉) · J. Mäkinen · J. Näränen
Finnish Geospatial Research Institute, National Land Survey, Espoo, Finland
e-mail: arttu.raja-halli@nls.fi

M. Nordman
Finnish Geospatial Research Institute, National Land Survey, Espoo, Finland

Department of Built Environment, Aalto University, Espoo, Finland

International Association of Geodesy Symposia,
https://doi.org/10.1007/1345_2026_332, © The Author(s) 2026

contribution to global sea level. To infer GIA-related crustal dynamics from gravimetry, it is necessary to isolate gravity signals caused by other geophysical processes, including atmospheric pressure variations, hydrological changes, and ocean tidal loading (OTL). Among these, OTL is a major contributor in polar regions, where ocean tide models may still exhibit uncertainties. Improved knowledge of Southern Ocean tides enhances geodetic corrections and contributes to the understanding of ice–ocean interactions and ice-shelf melt processes (Hausmann et al. 2020).

Ocean tides, caused primarily by the gravitational attraction of the Moon and the Sun, produce periodic elastic deformation of the Earth's crust and variation in gravity, collectively referred to as ocean tidal loading (OTL). These periodic effects can be detected in high-precision geodetic measurements with gravimeters and GNSS (Global Navigation Satellite Systems), even at inland locations. At Aboa, the gravimetric OTL signal reaches ~20 μGal (1 μGal = 10^{-8} m/s^2) peak-to-peak and is clearly visible in the AG data. AG measurements, and terrestrial gravimetric measurements in general, on the Antarctic continent are scarce, and Aboa is one of the few locations with repeated AG measurements.

While open-ocean tides are generally well predicted, coastal and shallow-water regions remain challenging due to complex dynamics. The Antarctic region poses additional challenges due to sparse in-situ observations for model assimilation (Padman et al. 2018). Uncertainties in sub-ice-shelf bathymetry and grounding line position further contribute to model uncertainty (Le Merle et al. 2024; Freer et al. 2023).

Gravity measurements have been successfully used to assess ocean tide models in both global and polar settings (e.g., Bos et al. 2002; Baker and Bos 2003). Several studies have investigated the performance of global and regional ocean tide models in Antarctica using gravity and GNSS observations. Early tidal gravity observations from the South pole were presented by Slichter et al. (1979), Agnew (1995) and Bos et al. (2000), and from Dronning Maud Land by Dietrich et al. (1995). Since then, gravimetry has been used for tidal research in Antarctic regions by several research groups. Doi et al. (2009) performed tidal gravimetry at Vostok Station. King and Padman (2005) and King et al. (2011) compared multiple ocean tide models with GNSS and gravity data, identifying significant shortcomings in many models and highlighting the lack of observational constraints in polar regions. Their results suggested that the TPXO6 model (Egbert and Erofeeva 2002) provided the best overall agreement. Relative gravimetry was subsequently used as a complementary tool to GNSS to validate TPXO6.2 at Belgrano II and San Martín stations (Scheinert et al. 2007, 2008, 2012). Kim et al. (2011) combined superconducting gravimeter, tide gauge, and bottom-pressure observations at Syowa Station and found TPXO7.1 to yield the smallest residuals. More recently, Sun et al. (2022) evaluated several models in the Antarctic Ocean, using GNSS, tide gauge, and satellite altimetry data, identifying TPXO9 as the most accurate around the Weddell Sea. However, Sun et al. (2022) had only a few in-situ observations from Dronning Maud Land and did not have the most recent model generations in their analysis. Since these studies, several models have been updated with improved polar coverage. Here, we analyse the performance and suitability of updated ocean tide models for correcting OTL in absolute gravity data from Aboa. Unlike most previous OTL validation efforts, which rely on GNSS or relative gravimetry, we use repeated AG measurements at Aboa. Repeated AG measurements can help constrain local vertical motion and gravity changes associated with GIA, providing a rare long-term observational anchor in Dronning Maud Land. To our knowledge, the most recent global and regional tide models have not previously been compared against gravity observations in Western Dronning Maud Land. This makes Aboa an important test site for assessing model performance and for improving the reliability of OTL corrections in high-latitude gravimetry, while providing an independent benchmark for modern global and regional tide models in coastal East Antarctica.

The paper is organized as follows: Sect. 2 describes the study site, gravity data, ocean tide models, and methodology; Sect. 3 presents the results; Sect. 4 discusses the findings; and Sect. 5 summarizes the conclusions.

2 Data and Methods

2.1 Aboa Station

The study site is the Finnish Antarctic research station Aboa, located in Dronning Maud Land at 73° 2′ 37″ S, 13° 24′ 24″ W. Aboa is situated on the slope of Basen nunatak – a mountain protruding through the surrounding glacier – approximately 200 m above the glacier surface and 470 m above sea level. The station lies about 15 km from the grounding line of the Riiser-Larsen Ice Shelf and roughly 110 km from the open ocean (see map in Fig. 1).

2.2 Absolute Gravity Measurements

Absolute gravity measurements at Aboa are campaign based and conducted during the austral summer. Measurements are performed in a temperature-stabilized laboratory on a concrete pillar anchored to the basaltic bedrock. The height of the gravity point is 462 m above sea level.

Absolute gravity observations at Aboa began in 1994, with several campaigns conducted since; detailed descrip-

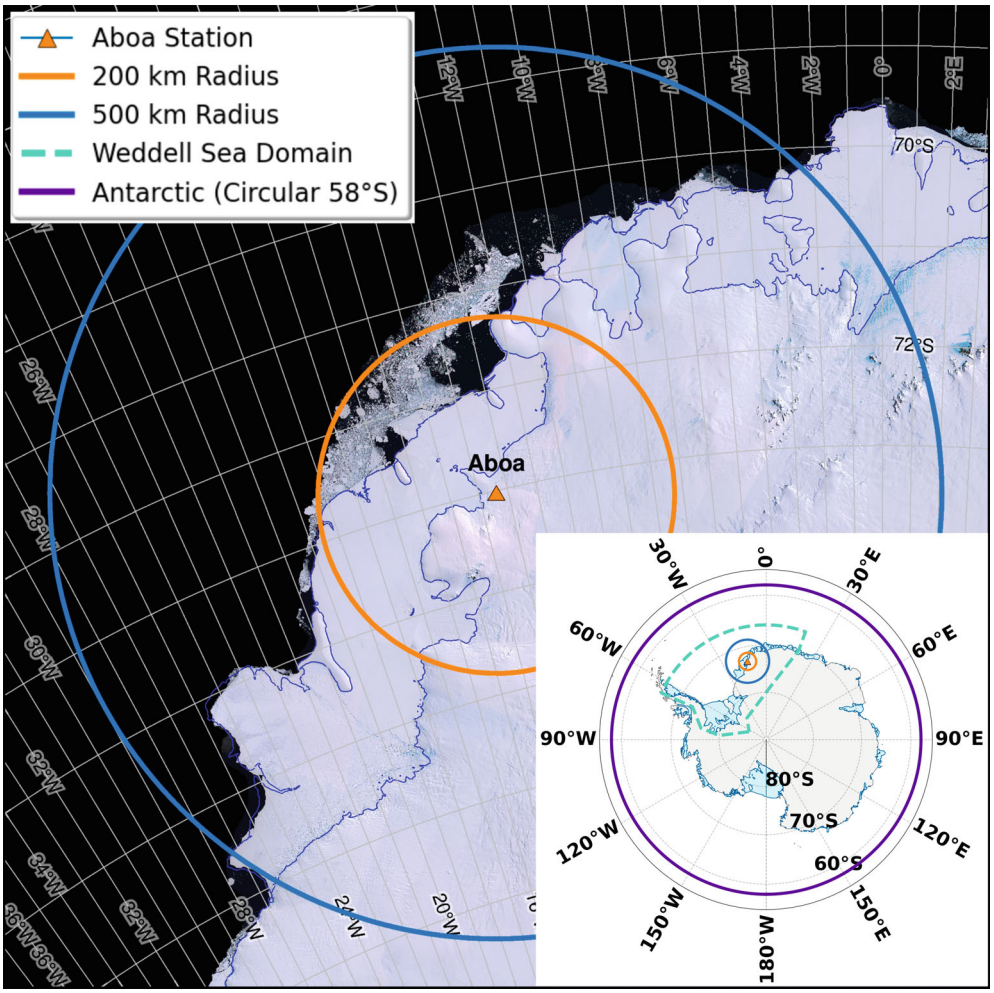

Fig. 1 Study site. Location of the Aboa station shown with grounding line and shelf ice boundary (BedMachine V3, Morlighem 2022 together with bounding lines used in the SPOTL computations for regional domains. (Satellite image Scambos et al. 2007, Haran et al. 2021)

tions of the measurement setup and earlier data analyses are given in Mäkinen et al. (2007) and Näränen et al. (2026).

In this study, we use AG data acquired with the FG5X-221 gravimeter during the 2024 campaign (23 January 2024–6 February 2024). Raw drop measurements were collected and processed using the g9 software (Micro-g LaCoste 2012). Each gravity set value is computed as the average of 50 individual drops made at 10 s intervals, resulting an effective integration time of ~500 s for each set value. Successive sets are separated by a pause resulting in a final sampling interval of ~30 min.

Two independent gravity time series were analysed: (1) 23 January 2024, 17:20 UT – 29 January 2024, 13:50 UT, comprising 282 gravity sets, and (2) 31 January 2024, 21:41 UT – 6 February 2024, 13:41 UT, comprising 273 gravity sets.

2.2.1 Gravity Data Processing

Only instrumental corrections were applied in g9 (Näränen et al. 2026). A statistical uncertainty estimate for each set is based on drop scatter. For the analysis the gravity variation was estimated as:

$$\Delta g(t) = g_{set}(t) - ST(t) + \alpha \Delta \rho_{AP} - OTL(t), \quad (1)$$

where $g_{set}(t)$ is the gravity set value, time-stamped at the midpoint of the 500 s drop sequence. Therefore, all tidal models were averaged over the same time window before subtraction. ST(t) is the solid Earth tide, including polar motion and length-of-day (LOD) effects, and $\alpha \Delta \rho_{AP}$ is the atmospheric correction computed with an admittance factor $\alpha = -0.3$ μGal/hPa. Effects from non-tidal loading and local mass variations were neglected. The objective is to

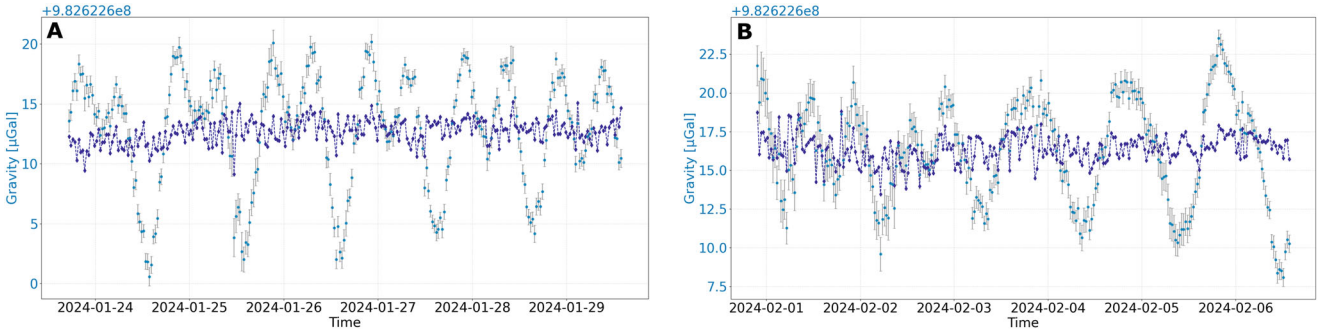

Fig. 2 Absolute gravity set values (in light blue) of week 1 (**a**. left) and week 2 (**b**. right) with Earth tide removed. Instrumental error bars (in grey) are one-sigma. In darker blue the residual values after correcting for best fitting ocean tide loading model. Best fit models: first week DTU23 + CATS2008v2023 (region "Antarctic"), with cRMS = 1.00 μGal. Second week TPXO10-atlas-V2 + CATS2008v2023 (200 km region), with cRMS = 0.91 μGal

identify the modelled $OTL(t)$ that minimizes the residual gravity signal $\Delta g(t)$ in the root-mean-square (RMS) sense, by finding the smallest:

$$cRMS = \sqrt{\frac{1}{N}\sum_{i=1}^{N}(r_i - \overline{r})^2}, \tag{2}$$

where r_i are gravity residuals and $\overline{r}$ is the mean of the gravity residual.

The solid Earth tide ST(t) was computed using the *Predict* module of ETERNA-X-v80 (Schüller 2015, 2020) using the DEHANT–DEFRAIGNE–WAHR non-hydrostatic inelastic Earth model (DDW-NHi, Dehant et al. 1999) and the Hartmann and Wentzel (1995) tidal potential. The prediction includes the 14 dominant wave groups (Mm, Mf, Q1, O1, P1, K1, N2, M2, S2, K2, M3, M4, M5, M6), as well as pole tide and LOD effects following the IERS conventions (IERS 2022). After removal of the solid Earth tide and atmospheric contributions, the remaining signal in $\Delta g(t)$ is dominated by ocean tidal loading, with a peak-to-peak amplitude of approximately 20 μGal (Fig. 2a, b).

For an independent comparison, the gravity data were also processed using the g9 internal corrections, which apply solid Earth tides, polar motion, and OTL based on the built-in FES2004 tidal constituents (Micro-g LaCoste 2012).

2.3 Ocean Tide Models

We compare the FES2004, the IERS standard for OTL corrections (Petit and Luzum 2013) and routinely used in g9 processing, and four other global models: DTU23 (Andersen 2023; Andersen et al. 2023), EOT20 (Hart-Davis et al. 2021a, b), FES2022b (Carrere et al. 2022; Lyard et al. 2026) and TPXO10-atlas-v2 (Egbert and Erofeeva 2002). DTU23 and EOT20 combine FES2014 (Carrere et al. 2016; Lyard et al. 2021) with improved satellite altimetry coverage in the polar regions. FES2022b offers higher resolution and better coastal bathymetry, and TPXO10-atlas-v2 incorporates tide gauge and Cryosat-2 data for polar coverage. We also include the high-resolution regional Antarctic model CATS2008v2023 (referred as CATS2023) (Howard et al. 2019, 2024), featuring 2 km resolution, refined coastlines, and scaling for ice shelf flexure near grounding lines. The CATS2023 extends south from latitude ~40°S and is bound to TPXO-model at the open ocean boundary. Model details are shown in Table 1.

Table 1 Ocean tide models evaluated in the study. Model classification: Empirical (E) – based on harmonic analysis of altimetry data; Hydrodynamic (HD) – numerical solution of physical tide equations; Data-assimilated (A) – hydrodynamic model constrained by altimetry/tide gauge observations. Spatial resolution shows the grid spacing of the model. We have interpolated CATS2008v2023 to a geographical grid of 3′ × 1.5′ (longitude × latitude) using bilinear interpolation

Model	Type	Spatial resolution
FES2004	Hydrodynamic	1/8°
FES2022b	Hydrodynamic + data assimilation	1/25°
TPXO10 Atlas v2	Data assimilated	1/30°
DTU23	Empirical	1/30°
EOT20	Empirical	1/8°
CATS2008v2023	Hydrodynamic	2 km, 3′ × 1.5′, 40°S–90°S

2.4 Ocean Tidal Loading

The ocean tide at a given latitude and longitude can be physically characterized, for each tidal constituent k (e.g., M2, S2, K1, O1) by an amplitude A_k and phase φ_k. For loading computations, the tidal height h_k is convenient to express by using a complex harmonic representation

$$h_k = h_{\mathrm{Re},k} + i h_{\mathrm{Im},k} = A_k e^{i\varphi_k}, \tag{3}$$

where $h_{\mathrm{Re},k}$ and $h_{\mathrm{Im},k}$ are the in-phase (real) and quadrature (imaginary) components of the complex tidal constant. These components are related to the conventional amplitude and phase parameters by:

$$A_k = \sqrt{{h_{\mathrm{Re},k}}^2 + {h_{\mathrm{Im},k}}^2}, \tag{4}$$

$$\varphi_k = atan2\left(h_{\mathrm{Im},k}, h_{\mathrm{Re},k}\right). \tag{5}$$

The ocean tide models used in the study were downloaded from the model providers either in amplitude-phase form (A_k, φ_k) or as complex components ($h_{\mathrm{Re,k}}$, $h_{\mathrm{Im,k}}$) for a regular latitude and longitude grid. For loading analysis all model grids were converted to $h_{\mathrm{Re,k}}$ and $h_{\mathrm{Im,k}}$ (in mm) with phases in Greenwich convention with positive lags.

We compute the OTL using the SPOTL software package (Agnew 2012), which implements the Green's function convolution method (Farrell 1972; Jentzsch 1997; Agnew 2012). In brief, the method integrates the product of the complex tidal height and the appropriate Green's function over the globe to obtain the total gravity effect at a specified location.

We used the precomputed Green's functions in SPOTL distribution for the Gutenberg–Bullen Model A (with the top 1,000 km replaced by oceanic crust and mantle structure; Harkrider 1970) in the reference frame of the solid Earth center of mass. Kim et al. (2011) showed that variations in Earth model choice lead to differences of a few percent in loading amplitudes. However, comparison of alternative Earth models is out of scope for this study.

For each tide model, synthetic loading harmonic constants $h_{k,\,LOAD}$ (amplitude A_k in μGal and local phase φ_k in degrees) were computed for eight principal diurnal and semidiurnal constituents (M2, S2, N2, K2, K1, P1, O1, Q1). For comparison with gravity measurements, we generate synthetic loading time series $OTL(t) = \Delta g_{LOAD}$ using SPOTL packages harprp and hartid. To ensure consistency with the gravity observations, which represent averages over a ~500 s drop sequence, the modeled loading values were averaged over the same time window and referenced to the midpoint of each gravity set epoch before comparing them with the measurements.

2.4.1 Evaluation of Ocean Tidal Loading Models

The total $OTL(t)$ was computed as the sum of (i) the global contribution from each tested global ocean tide model and (ii) the regional contribution obtained from the high-resolution Antarctic tide model CATS2008v2023. SPOTL's merging of regional and global solutions allows evaluation of regional refinement effects while retaining far-field coverage. The loading computations use SPOTL's land-sea mask which in the Antarctic region is based on GMT 3.0 (General Mapping Tools, Wessel and Smith 1996) basemap refined with Antarctic Digital Database grounding line information (see Agnew 2012 for details). The grounding line is defined in 1/64° resolution and closely agrees with more recent grounding line estimates from BedMachine v3 (Morlighem 2022) and Bedmap2 (Frémand et al. 2023); comparison not shown here.

The regional contribution was computed within four spatial domains surrounding Aboa (see Fig. 1), ranging from circum-Antarctic to strictly local scales:

1. Antarctic-wide region, "Antarctic": covering the Antarctic continent and the Southern Ocean south of latitude 58°S (Fig. 1, dark magenta line).
2. Intermediate region, "Weddell": a smaller region bounded longitudinally by the Antarctic Peninsula (~65°W) and 20°E, and extending from the Antarctic coast to north up to latitude 66°S. This region corresponds approximately to the southern limit of TOPEX/Poseidon altimetry used in several global models (Fig. 1, dashed light green line).
3. 500-km radius: a spherical area extending 500 km from Aboa (Fig. 1, blue line).
4. 200-km radius: a spherical area extending 200 km from Aboa. Mainly covered with shelf ice (Fig. 1, orange line).

OTL was recomputed independently for each region to test sensitivity to spatial extent and compare model behavior at smaller scales.

3 Results

3.1 Differences Between Models

For the inter-model comparison, we compare the model solutions only within the regional domains. The complex loading vectors $h_{k,LOAD} = A_k e^{i\varphi_k}$ (Eq. 3) for each model and constituent are shown in Fig. 3a–d. Within the smallest area of 200 km we find clear variability in the tidal constituents which increases only slightly when larger areas are considered. The largest differences occur in the semidiurnal constituents M2 and S2 and between FES2004 and FES2022b. Difference in the $h_{k,\,LOAD}$ for M2 constituent is 0.25 μGal between FES2004 and FES2022b. In S2, the FES2022b shows largest variation in $h_{k,\,LOAD}$ compared to the other models, deviation being 0.18–0.22 μGal. Other constituents show agreement below 0.1 μGal. Largest differences are found in the K1 constituent for the FES2004 and EOT20 in respect to other models being ~0.07 μGal for FES2004 and ~0.08 μGal for the EOT20. Expanding the regional domain to 500 km, K1 shows a difference of 0.10 μGal between FES2004 and other models, while M2 differences between FES2004 and FES2022b increases to 0.29 μGal. For S2, FES2022b stands out, differing from the rest by 0.22–0.24 μGal. These results indicate that

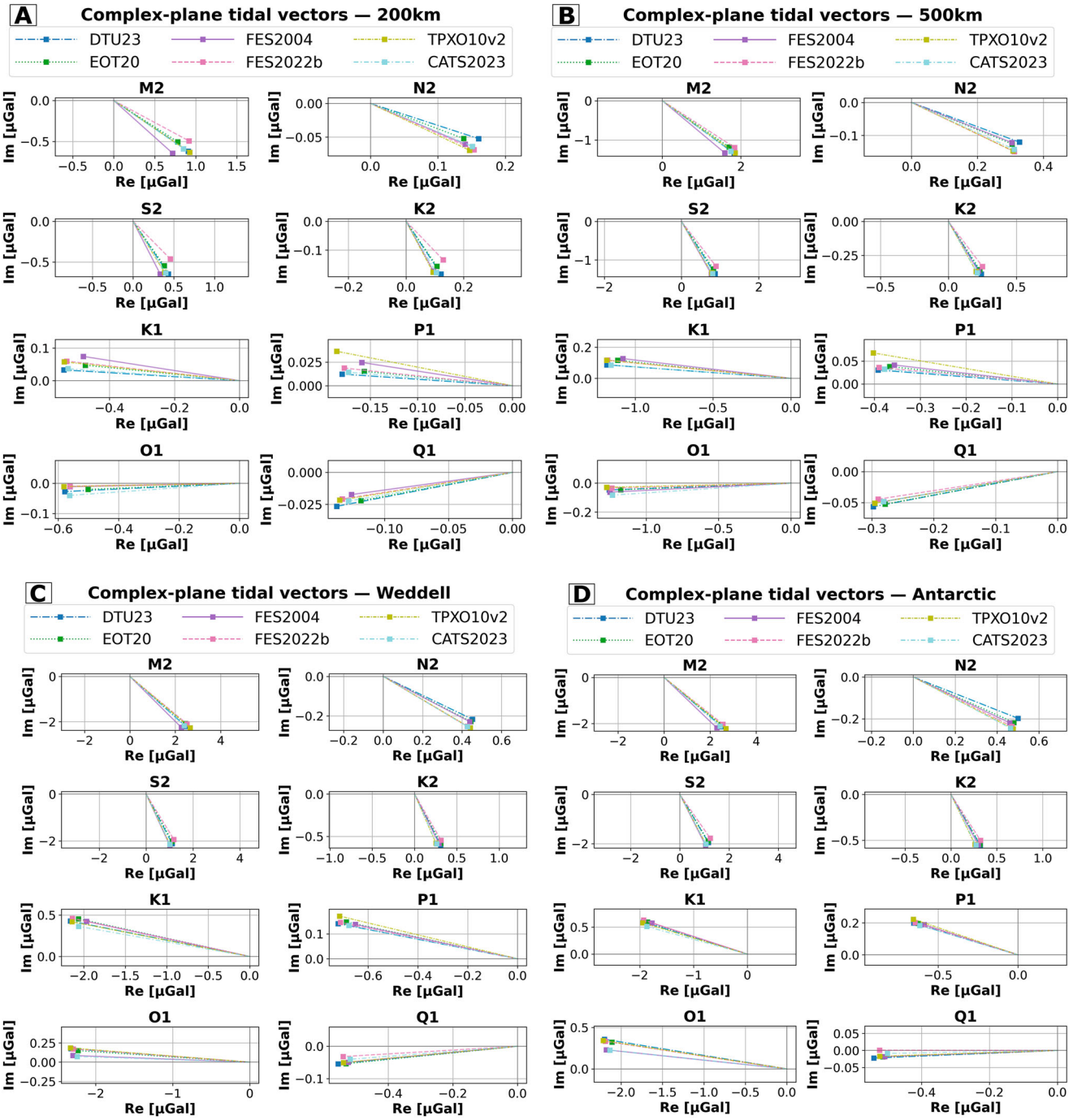

Fig. 3 Complex harmonic constants of OTL at Aboa for selected tidal constituents derived from different ocean tide models. Real and imaginary components (μGal) are plotted on the x- and y-axes, respectively. Panels show loading computed for four regional domains used in the study: (**a**) 200 km around Aboa, (**b**) 500 km around Aboa, (**c**) "Weddell" region, and (**d**) "Antarctic" region. Vector magnitude corresponds to loading amplitude and vector orientation to phase

differences between models are dominated by the near-field contributions within a few hundred kilometers of the station, and that the discrepancies grow modestly with increasing regional extent, particularly for M2 and S2. Most of the total variation arises from the difference in amplitude and less in the phase. This can be also seen in the complex vectors of each constituent shown in Fig. 3a–d.

The differences between FES2004 and EOT20 and more recent models is at least partially explained with the improved assimilation data, placement of grounding

lines, treatment of ice shelves, and representation of narrow coastal cavities. The newer models DTU23, FES2022b, TPXO-atlas-v2 and CATS2008v2023 align much better with the BedMachine v3 grounding line as well as with the SPOTL land-sea mask. In addition to the representation of the grounding line, the recent models come with higher-resolution grids (Table 1).

3.2 Ocean Tidal Loading Correction of Absolute Gravity

For the first week, the configuration with the smallest cRMS (1.00 μGal) was CATS2008v2023 within the Antarctic region together with DTU23 for the global domain (Fig. 2a). For the second week, configuration with the smallest cRMS (0.91 μGal) combined CATS2008v2023 within 200 km radius together with TPXO10-atlas-v2 for the global domain (Fig. 2b). Although combined solutions consistently outperformed the global-only models, the difference between the best and worst performing solutions were small, with residual cRMS values between 1.00–1.05 μGal for the first week and 0.91–0.97 μGal for the second week. In addition to the weekly cRMS values, we evaluated the relative performance of each model solution by computing the deviation of the cRMS from the quadratic mean (q-mean, i.e., root-mean-square) of the cRMS values of all models for a given week, as well as for the combined two-week period. Deviation of the cRMS from the weekly q-mean highlights how each model performs with respect to the average of all models, while removing week-to-week offsets unrelated to ocean tidal loading. The comparison highlights the spread and stability of the model performance between the two measurement periods. The combined two-week comparison provides relative measure of model consistency and does not necessarily identify the single best performing model in terms of agreement with absolute gravity data. Negative deviation indicates models whose residual variability is smaller than the average of all models (DTU23, EOT20 and TPXO10-atlas-v2), while positive values indicate larger-than-average cRMS (global-only solutions). FES2004 showed the largest deviations from the average of all models. The results of the comparison are shown in Fig. 4.

We also compared the resulting gravity residuals to a residual computed with the g9 internal solid Earth and FES2004 tidal corrections. Our best model solution (DTU23 + CATS2008v2023) reduced the residual cRMS by 0.14 μGal (≈12%) for the week 1 and for the week 2 the best solution (TPXO10-atlas-v2 + CATS2008v2023) reduced the cRMS by 0.25 μGal (≈22%) compared to the residual produced with g9. This clearly indicates the improvements in the modern models and the benefit of utilizing a regional

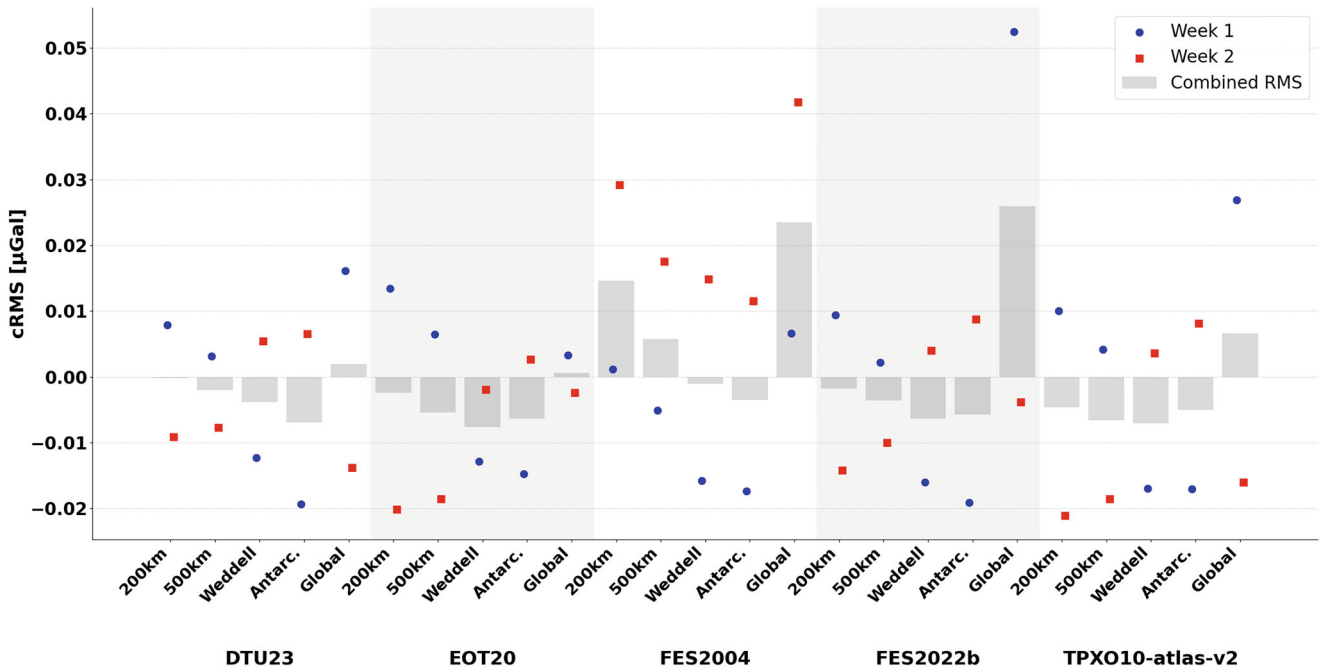

Fig. 4 Deviation of model cRMS from the quadratic mean across models. Differences between each model's weekly cRMS and the quadratic mean of the cRMS values from all models are shown for Week 1, Week 2, and the combined 2-week period. Each solution represents either a global-only model or a combination of a global model (indicated along the lower axis) with the CATS2008v2023 regional model applied in the local domain (listed along the x-axis). Blue circles denote Week 1 results, red squares Week 2 results, and the bars represent the combined 2-week evaluation

model in the loading analysis. In addition, the comparison to g9 solution might be partially affected by the differences in the land-sea mask used for the computation of the harmonic constants. The underlying land-sea mask used within g9 is not-known. Notably, all model solutions computed with SPOTL – including the global-only models – indicated a generally high level of model consistency producing cRMS values below 1 μGal for the second week.

4 Discussion

This study provides one of the first terrestrial gravity-based evaluations of recent global and regional ocean tide models in Western Dronning Maud Land. Despite the short duration of the two AG campaigns, the results demonstrate that all models perform at a level consistent with the nominal uncertainty of absolute gravity measurements. This is an encouraging outcome, indicating that modern global ocean tide models, together with the high-resolution CATS2008v2023 solution, provide broadly consistent OTL corrections at Aboa, a region where observational data for model assimilation is sparse. The analysis also shows that including the regional model CATS2008v2023 improves local loading estimate, which is important for future gravimetric studies in coastal Antarctica. However, there are some limitations. First, the short duration of our absolute gravity (AG) campaigns (~6 days each) does not allow a full spectral tidal analysis. As a result, our approach is limited to computing synthetic tidal loading for the given ocean tide models and minimizing the gravity residuals after OTL correction. Second, the differences between model solutions proved to be small, preventing us from really distinguishing between models based on these short campaigns alone. An additional source of uncertainty arises from the synthetic solid Earth tide correction computed with ETERNA and applied to the AG time series. Any deficiencies in the body tide correction can leak into the AG – OTL analysis and affect the apparent performance of the ocean tide models. This leakage is difficult to quantify for short datasets and may partly explain the week-to-week variability we observe. Given this and considering the additional non-tidal signals present in the residuals, our short campaigns do not allow a robust discrimination between models. Incorporating longer time series is therefore essential. Future work will include integrating data from earlier AG campaigns at Aboa, together with continuous GNSS observations, to widen the temporal coverage and reduce aliasing of non-tidal signals. These measurements could be complemented with GNSS measurements directly on the ice shelf close to the station to provide direct measurement on the tidal movement of the underlying water and ice shelf. Finally, we note that uncertainties inherent in the ocean tide models themselves were not explicitly included in this study.

5 Conclusions

We have compared the performance of five global ocean tide models (FES2004, FES2022b, EOT20, DTU23, TPXO10-atlas-v2) and one regional ocean tide model (CATS2008v2023) by estimating ocean tidal loading at Aboa, Antarctica. For each model, we computed harmonic constants for eight diurnal and semidiurnal tidal constituents and evaluated model performance by estimating the cRMS of residuals after correcting absolute gravity measurements for computed OTL. All models produce gravity residual cRMS values within 1.0 ± 0.2 μGal. Inclusion of the regional Antarctic model CATS2008v2023 improves the residual. The largest inter-model differences were found between FES2004 and FES2022b for the M2 and S2 constituents, reaching 0.25 μGal for M2 and 0.22 μGal for S2 within a 200 km radius of Aboa. Overall, these results indicate that modern global and regional tide models provide improved OTL corrections for short-term AG campaigns, with regional models providing additional improvement in near-field tidal effects. These results highlight the need for extended gravity and geodetic measurements to refine tidal models and better characterize local mass and crustal dynamics in Antarctica. We will perform such measurements in the upcoming scientific expedition to Aboa. The current research provides a valuable starting point for the planned extended measurement campaigns.

Acknowledgements The gravity data was collected with the support by the Finnish Antarctic Research Programme FINNARP. The FES2022 Tide product was funded by CNES, produced by LEGOS, NOVELTIS and CLS and made freely available by "AVISO". CNES, 2024. FES2022 (Finite Element Solution) Tidal model (Version 2024) [Data set]. CNES. https://doi.org/10.24400/527896/A01-2024.004. PolarToolkit (Tankersley 2024) was used to generate the map in Fig. 1.

Competing Interests The author(s) has no competing interests to declare that are relevant to the content of this manuscript.

Funding This research was partially funded by the Research Council of Finland (decision number 364868).

References

Agnew DC (1995) Ocean-load tides at the South Pole: a validation of recent ocean-tide models. Geophys Res Lett 22(22):3063–3066. https://doi.org/10.1029/95GL03074

Agnew DC (2012) SPOTL: some programs for ocean-tide loading. SIO Technical Report. Scripps Institution of Oceanography. https://igppweb.ucsd.edu/~agnew/Spotl/

Andersen OB (2023) DTU23 Global Ocean Tide model (DTU23_OceanTide). Technical University of Denmark. Dataset. https://doi.org/10.11583/DTU.23828874.v1

Andersen OB, Rose SK, Hart-Davis MG (2023) Polar ocean tides – revisited using CryoSat-2. Remote Sens 15(18):4479. https://doi.org/10.3390/rs15184479

Baker TF, Bos MS (2003) Validating Earth and ocean tide models using tidal gravity measurements. Geophys J Int 152(2):468–485. https://doi.org/10.1046/j.1365-246X.2003.01863.x

Bilker-Koivula M, Mäkinen J, Ruotsalainen H, Näränen J, Saari T (2021) Forty-three years of absolute gravity observations of the Fennoscandian postglacial rebound in Finland. J Geod 95(2):24. https://doi.org/10.1007/s00190-020-01470-9

Bos MS, Baker TF, Lyard FH, Zürn WE, Rydelek PA (2000) Long-period lunar Earth tides at the geographic South Pole and recent models of ocean tides. Geophys J Int 143(2):490–494. https://doi.org/10.1046/j.1365-246X.2000.01260.x

Bos MS, Baker TF, Røthing K, Plag H-P (2002) Testing ocean tide models in the Nordic seas with tidal gravity observations. Geophys J Int 150(3):687–694. https://doi.org/10.1046/j.1365-246X.2002.01729.x

Carrere L, Lyard F, Cancet M, Guillot A, Picot N (2016) FES2014: a new tidal model – validation results and perspectives for improvements. In: ESA living planet conference, Prague (conference presentation)

Carrere L et al (2022) A new barotropic tide model for global ocean: FES2022. In: OSTST 2022. https://doi.org/10.24400/527896/a03-2022.3287

Dehant V, Defraigne P, Wahr J (1999) Tides for a convective Earth. J Geophys Res 104(B1):1035–1058

Dietrich R, Liebsch G, Dittfield HJ, Noack G (1995) Ocean tide and attempt of Earth tide recordings at Schirmacher Oasis/Dronning Maud Land (Antarctica). In: Proceedings of 12th international symposium on Earth tides. Science Press, Beijing, New York

Doi K, Shibuya K, Wendt A, Dietrich R, King M (2009) Tidal gravity variations revisited at Vostok Station, Antarctica. Polar Sci 3(1):1–12. https://doi.org/10.1016/j.polar.2008.11.001

Egbert GD, Erofeeva SY (2002) Efficient inverse modeling of barotropic ocean tides. J Atmos Ocean Technol 19(2):183–204. https://doi.org/10.1175/1520-0426(2002)019

Farrell WE (1972) Deformation of the Earth by surface loads. Rev Geophys 10:761–797

Freer BID, Marsh OJ, Hogg AE, Fricker HA, Padman L (2023) Modes of Antarctic tidal grounding-line migration revealed by ICESat-2 laser altimetry. Cryosphere 17:4079–4101. https://doi.org/10.5194/tc-17-4079-2023

Frémand AC, Fretwell P, Bodart JA, Pritchard HD, Aitken A, Bamber JL, Bell R, Bianchi C, Bingham RG, Blankenship DD, Casassa G, Catania G, Christianson K, Conway H, Corr HFJ, Cui X, Damaske D, Damm V, Drews R et al (2023) Antarctic Bedmap data: Findable, Accessible, Interoperable, and Reusable (FAIR) sharing of 60 years of ice bed, surface, and thickness data. Earth Syst Sci Data 15(7):2695–2710. https://doi.org/10.5194/essd-15-2695-2023

Haran T, Bohlander J, Scambos TA, Painter T, Fahnestock M (2021) MODIS mosaic of Antarctica 2008–2009 (MOA2009) image map, version 2. https://doi.org/10.5067/4ZL43A4619AF

Harkrider D (1970) Surface waves in multilayered elastic media (2): higher mode spectra and spectral ratios from point sources in plane-layered earth models. Bull Seismol Soc Am 60:1937

Hart-Davis M, Piccioni G, Dettmering D, Schwatke C, Passaro M, Seitz F (2021a) EOT20 – a global empirical ocean tide model from multi-mission satellite altimetry. SEANOE. https://doi.org/10.17882/79489

Hart-Davis MG, Piccioni G, Dettmering D, Schwatke C, Passaro M, Seitz F (2021b) EOT20: a global ocean tide model from multi-mission satellite altimetry. Earth Syst Sci Data 13(8):3869–3884. https://doi.org/10.5194/essd-13-3869-2021

Hartmann T, Wentzel H-G (1995) The HW95 tidal potential catalogue. Geophys Res Lett 22(24):3553–3556. https://doi.org/10.1029/95GL03324

Hausmann U, Sallée J-B, Jourdain NC, Mathiot P, Rousset C, Madec G et al (2020) The role of tides in ocean-ice shelf interactions in the Southwestern Weddell Sea. J Geophys Res Oceans 125(6):e2019JC015847. https://doi.org/10.1029/2019JC015847

Howard SL, Erofeeva S, Padman L (2019) CATS2008: circum-Antarctic tidal simulation version 2008. U.S. Antarctic Program Data Center. https://doi.org/10.15784/601235

Howard SL, Greene CA, Padman L, Erofeeva S, Sutterley T (2024) CATS2008_v2023: circum-Antarctic tidal simulation 2008, version 2023. U.S. Antarctic Program Data Center. https://doi.org/10.15784/601772

International Earth Rotation and Reference System Service (IERS) (2022). http://hpiers.obspm.fr/eop-pc/index.php?index=C04&lang=en

Jentzsch G (1997) Earth tides and ocean tidal loading. In: Wilhelm H, Zürn W, Wenzel H-G (eds) Tidal phenomena. Springer, pp 145–171

Kim T-H, Shibuya K, Doi K, Aoyama Y, Hayakawa H (2011) Validation of global ocean tide models using the superconducting gravimeter data at Syowa Station, Antarctica, and in situ tide gauge and bottom-pressure observations. Polar Sci 5:21–39. https://doi.org/10.1016/j.polar.2010.11.001

King MA, Padman L (2005) Accuracy assessment of ocean tide models around Antarctica. Geophys Res Lett 32:L23608. https://doi.org/10.1029/2005GL023901

King MA, Padman L, Nicholls KW, Clarke PJ, Gudmundsson H, Kulessa B, Shepherd A (2011) Ocean tides in the Weddell Sea: new observations on the Filchner-Ronne and Larsen C ice shelves and model validation. J Geophys Res 116:C06006. https://doi.org/10.1029/2011JC006949

Le Merle E, Belot C, Fouchet E, Cancet M, Andersen OB, Lyard F, Moholdt G et al (2024) ALBATROSS: advancing Southern Ocean tide modelling with high resolution and enhanced bathymetry. Pol Sci 42:101124. https://doi.org/10.1016/j.polar.2024.101124

Lyard FH, Allain DJ, Cancet M, Carrère L, Picot N (2021). FES2014 global ocean tide atlas: design and performance. Ocean Sci 17:615–649. https://doi.org/10.5194/os-17-615-2021

Lyard F, Carrere L, Fouchet E, Cancet M, Greenberg D, Dibarboure G, Picot N (2026) FES2022 a step towards a SWOT-compliant tidal correction. Manuscript in preparation

Mäkinen J, Amalwict M, Shibuya K, Fukuda Y (2007) Absolute gravimetry in Antarctica: status and prospects. J Geodyn 43(3):339–357. https://doi.org/10.1016/j.jog.2006.08.002

Micro-g LaCoste (2012) Micro-g LaCoste g9 user's manual. https://microglacoste.com/download/g9-users-manual/

Morlighem M (2022) MEaSUREs BedMachine Antarctica (NSIDC-0756, version 3). [Dataset]. NASA National Snow and Ice Data Center Distributed Active Archive Center, Boulder. https://doi.org/10.5067/FPSU0V1MWUB6

Näränen J, Mäkinen J, Nordman M, Raja-Halli A (2026). Three decades of repeated absolute gravity measurements at the Finnish Antarctic Research Station Aboa. Pure Appl Geophys 183:137–157. https://doi.org/10.1007/s00024-025-03868-y

Padman L, Siegfried MR, Fricker HA (2018) Ocean tide influences on the Antarctic and Greenland ice sheets. Rev Geophys 56:142–184. https://doi.org/10.1002/2016RG000546

Petit G, Luzum B (2013) The 2010 reference edition of the IERS conventions. In: Altamimi Z, Collilieux X (eds) Reference frames for applications in geosciences (IAG symposia 138). Springer. https://doi.org/10.1007/978-3-642-32998-2_10

Scambos TA, Haran TM, Fahnestock MA, Painter TH, Bohlander J (2007) MODIS-based mosaic of Antarctica (MOA) datasets: continent-wide surface morphology and snow grain size. Remote Sens Environ 111(2–3):242–257. https://doi.org/10.1016/j.rse.2006.12.020

Scheinert M, Zakrajsek AF, Eberlein L, Marenssi S, Ghidella M, Dietrich R, Rülke A (2007) Gravimetry and GPS observations at Belgrano II station to test ocean tidal models. Rev Asoc Geol Argent 62:646–651

Scheinert M, Zakrajsek AF, Marenssi SA, Dietrich R, Eberlein L (2008) Tidal gravimetry in polar regions: an observation tool complementary to continuous GPS for validating ocean tide models. In:

Capra A, Dietrich R (eds) Geodetic and geophysical observations in Antarctica. Springer. https://doi.org/10.1007/978-3-540-74882-3_15

Scheinert M, Zakrajsek AF, Eberlein L, Dietrich R, Marenssi SA, Ghidella ME (2012) Gravimetric time series recording at the Argentine Antarctic stations Belgrano II and San Martín for the improvement of ocean tide models

Schüller K (2015) Theoretical basis for earth tide analysis with the new ETERNA34-ANA-V4.0 program. Bull Inf Marées Terr 149(1):12024–12061. http://maregraph-renater.upf.pf/bim/BIM/bim149.pdf

Schüller K (2020) Program system ETERNA-x et34-x-v80-* for earth and ocean tides analysis and prediction, documentation manual 01: theory. Technical report, institution. http://ggp.bkg.bund.de/eterna?download=7283

Slichter LB, Zürn W, Syrstad E, Knopoff L, Smythe WD, Uffelman H (1979) Long-period gravity tides at the South Pole. J Geophys Res 84(B11):6207–6212. https://doi.org/10.1029/JB084iB11p06207

Sun W, Zhou W, Zhou D, Sun Y (2022) Advances and accuracy assessment of ocean tide models in the Antarctic Ocean. Front Earth Sci 10. https://doi.org/10.3389/feart.2022.757821

Tankersley MD (2024) PolarToolkit: python tools for convenient, reproducible, and open polar science. J Open Source Softw 9(100):6502. https://doi.org/10.21105/joss.06502

van Dam T, Francis O, Wahr J, Khan SA, Bevis M, van den Broeke MR (2017) Using GPS and absolute gravity observations to separate the effects of present-day and Pleistocene ice-mass changes in South East Greenland. Earth Planet Sci Lett 459:127–135. https://doi.org/10.1016/j.epsl.2016.11.01

Wessel P, Smith WHF (1996) A global, self-consistent, hierarchical, high-resolution shoreline database. J Geophys Res 101:8741–8743